RSC Advances

PAPER

View Article Online
View Journal | View Issue

Cite this: *RSC Adv.*, 2021, **11**, 7338

Impact of Al doping on a hydrothermally synthesized β-Ga_2O_3 nanostructure for photocatalysis applications

Sunjae Kim,[ab] Heejoong Ryou,[a] In Gyu Lee,[a] Myunghun Shin,[c] Byung Jin Cho[d] and Wan Sik Hwang*[ab]

Aluminum (Al)-doped beta-phase gallium oxide (β-Ga_2O_3) nanostructures with different Al concentrations (0 to 3.2 at%) are synthesized using a hydrothermal method. The single phase of the β-Ga_2O_3 is maintained without intermediate phases up to Al 3.2 at% doping. As the Al concentration in the β-Ga_2O_3 nanostructures increases, the optical bandgap of the β-Ga_2O_3 increases from 4.69 (Al 0%) to 4.8 (Al 3.2%). The physical, chemical, and optical properties of the Al-doped β-Ga_2O_3 nanostructures are correlated with photocatalytic activity *via* the degradation of a methylene blue solution under ultraviolet light (254 nm) irradiation. The photocatalytic activity is enhanced by doping a small amount of substitutional Al atoms (0.6 at%) that presumably create shallow level traps in the band gap. These shallow traps retard the recombination process by separating photogenerated electron–hole pairs. On the other hand, once the Al concentration in the Ga_2O_3 exceeds 0.6 at%, the crystallographic disorder, oxygen vacancy, and grain boundary-related defects increase as the Al concentration increases. These defect-related energy levels are broadly distributed within the bandgap, which act as carrier recombination centers and thereby degrade the photocatalytic activity. The results of this work provide new opportunities for the synthesis of highly effective β-Ga_2O_3-based photocatalysts that can generate hydrogen gas and remove harmful volatile organic compounds.

Received 2nd January 2021
Accepted 29th January 2021

DOI: 10.1039/d1ra00021g

rsc.li/rsc-advances

Introduction

Gallium oxide (Ga_2O_3) is a wide bandgap semiconductor with five polymorphs designated as α-, β-, γ-, δ-, and ε-phase.[1] Among them, β-Ga_2O_3 has been widely studied as a promising semiconductor material for power electronics and ultraviolet (UV) photodetectors due to its wide bandgap of ~4.9 eV (ref. 2–4) and its thermodynamic stability.[5] β-Ga_2O_3 is also considered an effective photocatalyst under ultraviolet-C (UVC) light irradiation for the generation of hydrogen[6–8] and removal of volatile organic compounds (VOCs).[9–12] β-Ga_2O_3 has a high redox potential, which is beneficial for photocatalytic reactions under photoexcitation conditions.[9,13] Its redox potential is higher than TiO_2, so it exhibits better photocatalytic performance than conventional TiO_2 photocatalysts. Meanwhile, the recombination of photogenerated electron–hole pairs is known to severely degrade photocatalytic efficiency;[14,15] when the electron–hole pairs recombine and the carrier concentrations become depleted, the photocatalytic reactions decrease as a consequence. Indeed, various approaches have been developed to suppress the recombination in Ga_2O_3-based photocatalysts.[16–23] Doping in photocatalysts is a method of suppressing the recombination process, which creates available energy states in the bandgap underneath the conduction band edge and/or above the valence band edge.[16–19] These additional energy levels in the forbidden bandgap can separate charged carriers and thereby retard the recombination process, allowing more charged carriers to diffuse in the surface and consequently enhances the photocatalytic reactions.[24,25] Thus far, reports have indicated that dopants in Ga_2O_3 have reduced the bandgap energy of Ga_2O_3, which reduce the benefits of the high redox potential effects that Ga_2O_3 posseses.[16–20,24–27] Therefore, it would be beneficial to apply a dopant atom that could increase the Ga_2O_3 bandgap with the dopant concentration. It has been reported that aluminum (Al) can increase the Ga_2O_3 bandgap upon doping.[28–30] Thus, Al doping in Ga_2O_3 semiconductors has been intensively studied to modulate the energy bandgap for power electronics and photodetectors.[28–30] However, the photocatalytic properties of Ga_2O_3 semiconductors have not yet been reported for various Al dopings. In this work, we analyze the effects of Al doping on hydrothermal synthesized β-Ga_2O_3

[a]*Department of Materials Engineering, Korea Aerospace University, Goyang, 10540, Republic of Korea. E-mail: whwang@kau.ac.kr*
[b]*Department of Smart Drone Convergence, Korea Aerospace University, Goyang, 10540, Republic of Korea*
[c]*Department of Electronics and Information Engineering, Korea Aerospace University, Goyang, 10540, Republic of Korea*
[d]*School of Electrical Engineering, Korea Advanced Institute of Science and Technology, Daejeon, 34141, Republic of Korea*

nanostructures for photocatalyst applications. The crystal structures, optical bandgap, and chemical states of the Al-doped Ga_2O_3 are investigated with different Al concentrations (0.0 to 3.2 at%), which are also correlated with the photocatalytic activity of Al-doped Ga_2O_3.

Experimental

Hydrothermal synthesis of Al-doped β-Ga_2O_3 nanostructures

First, 0.1 M gallium(III) nitrate hydrate ($Ga(NO_3)_3 \cdot xH_2O$) was dissolved in 50 mL of deionized (DI) water using a magnetic stirrer at room temperature, where the pH of the initial solution was 2.5. The pH value in the solution was adjusted to approximately 10 by adding an ammonium hydroxide solution ($NH_4(OH)$ 28 vol% in H_2O) which was necessary to form β-Ga_2O_3 nanostructures *via* a hydrothermal reaction.[26,27,31] To dope Al in the β-Ga_2O_3 nanostructures with different concentrations, different amounts of aluminum nitrate nonahydrate ($Al(NO_3)_3 \cdot 9H_2O$) (0.02, 0.064, 0.110, and 0.210 g for Al 0.6, 1.2, 2.2, and 3.2 at% concentrations, respectively) were added into the prepared solution. The pH value of the mixed solution was 10.34 for the intrinsic β-Ga_2O_3 nanostructures, and the value continued to decrease as the Al concentration increased, ultimately reaching 10.08 for the Al 3.2 at. %-doped β-Ga_2O_3 nanostructures. This pH value reduction was caused by the aluminum nitrate nonahydrate ($Al(NO_3)_3 \cdot 9H_2O$) in the mixed solution. The supersaturated mixed solution was transferred to a Teflon-lined stainless-steel autoclave, thermally treated at 140 °C for 10 h, and subsequently cooled down naturally to room temperature.[26,27,31] After the hydrothermal synthesis process, α-GaOOH nanostructures with different Al concentration were collected, washed three times with DI water, and then dried in an oven at 70 °C for 6 h. It is noted that α-GaOOH nanostructures were precipitated in dissolved solutions ($Ga(NO_3)_3 \cdot xH_2O$) with an ($NH_4(OH)$) alkali in this work, and it was reported that the α-GaOOH nanostructures were also precipitated in dissolved solutions ($Ga(NO_3)_3 \cdot xH_2O$) with other alkalis such as NaOH, KOH, $NaHCO_3$, and Na_2CO_3.[32] In addition, the morphologies of the GaOOH were found to have significantly different in terms of pH values.[33] Finally, Al-doped β-Ga_2O_3 nanostructures were obtained after annealing the Al-doped GaOOH nanostructures in an O_2 ambient at 1000 °C for 6 h. After each experiment set, approximately 500 mg of GaOOH was obtained with different Al concentrations. This was converted into about 450 mg of β-Ga_2O_3.

Characterization of Al-doped β-Ga_2O_3 nanostructures

The crystal structures and morphologies of the samples were characterized using a powder X-ray diffraction system (XRD, Rigaku SmartLAB, Tokyo, Japan) over the 2θ range with Cu Kα radiation ($\lambda = 0.15405$ nm) and using a field-emission scanning electron microscope (FESEM, JSM-7100F, JEOL, Peabody, MA, USA), respectively. The specific surface areas of the samples were measured *via* the Brunauer–Emmett–Teller (BET) method using a conventional flow apparatus (BELSORP-mini II, Osaka, Japan) with nitrogen adsorption at −196 °C. The chemical states of the elements presented on the sample surface were analyzed using X-ray photoelectron spectroscopy (XPS, Thermo Fisher Scientific, K-ALPHA+ System), which also determined the Al concentrations in the β-Ga_2O_3 nanostructures. The optical bandgaps of the samples were extracted using diffuse reflectance spectroscopy (DRS, SHIMADZU, SolidSpec-3700) *via* Tauc plots (direct bandgap model). Relative redox potential of the Al-doped β-Ga_2O_3 nanostructures was obtained from the optical bandgaps. The crystalline domain sizes of the Al-doped β-Ga_2O_3 nanostructures were subsequently estimated using the Scherrer equation[34] in eqn (1), which is inversely proportional to the total length of the grain boundaries (GBs).

$$\text{Domain size} = \frac{K\lambda}{\beta_{\text{size}} \cos\theta} \quad (1)$$

where K is a dimensionless shape factor of 0.9, λ is an X-ray wavelength of 0.15405 nm, β_{size} is the full width at half maximum (FWHM) of the XRD peaks, and θ is the Bragg angle.

Photocatalytic activity of Al-doped β-Ga_2O_3 nanostructures

The photocatalytic activity of the samples was evaluated *via* the degradation of a methylene blue (MB) solution, which is a model system. It was found that the MB oxidation is mainly driven by the OH radical that is generated due to the photocatalytic activity.[35] 4 mg of each sample was homogeneously dispersed in the 4 mL MB solution (1.56 mg L^{-1} in DI water), which was then exposed to the 6 W ultraviolet-C (UVC) lamp (UVG-11, Germany) with a wavelength center at 254 nm and 312 μW cm^{-2} for 10 min. After the β-Ga_2O_3 nanostructures were filtered through a syringe filter (0.45 μm), the absorbance of the MB solution was measured using UV-VIS spectrophotometers (UV-3600 plus, Shimadzu, Kyoto, Japan). An intact MB solution (without UVC exposure) was used as a control for comparison. The photocatalytic activity (%) of the Al-doped β-Ga_2O_3 nanostructures with different Al concentrations was defined using eqn (2).

$$\text{Photoctalytic activity} = \frac{C_i - C}{C_i}, \quad (2)$$

where C_i and C are the absorbances at $\lambda = 664$ nm from the intact MB solution and the UVC-exposed MB solution in the presence of Al-doped β-Ga_2O_3 nanostructures with different Al concentrations, respectively. The photogenerated electron–hole pairs in the Al-doped β-Ga_2O_3 nanostructures in the MB solution generated reactive oxygen species that eventually decomposed the MB.[36]

Redox potential (RP), surface area (SA), and oxygen deficiency defects (OD) were defined based on the extracted optical bandgap, the specific surface area value obtained through the BET analysis method, and O 1s spectra using XPS, respectively. Crystallographic defects (CD) and grain boundary-induced defects (GD) were respectively defined based on the average values of the intensity and domain size of the three (−401), (002), and (111) peaks obtained through XRD analysis.

Results and discussion

The X-ray diffraction patterns of the GaOOH and Al-doped Ga_2O_3 nanostructures are presented in Fig. 1(a). The intrinsic

Ga_2O_3 nanostructures were indexed to the monoclinic β-Ga_2O_3. The single phase was maintained without intermediate phases up to Al 3.2 at%, which was in agreement with previous results in which the maximum solid solubility of Al in the Ga_2O_3 was 80 at%.[37] The crystal structure and domain size of the Al-doped β-Ga_2O_3 were affected by the amounts of Al dopant, as shown in Fig. 1(b–d). In Fig. 1(b) and (c), the peak intensities of (−401), (002), and (111) decrease, and the peak positions shift toward a higher 2θ angle as the Al concentration increases. These results indicate that the Al dopants in the β-Ga_2O_3 nanostructures reduce the crystallinity degree and lattice constant of the β-Ga_2O_3 nanostructures, resulting in a maximum compressive strain as high as approximately 0.35% at the Al concentration of 3.2 at%. The 8% smaller radius of the Al^{3+} (57 ppm), which was substituted at the octahedral sites in the β-Ga_2O_3,[38] than that of the Ga^{3+} (62 ppm) caused these structural changes.[39] In addition, as seen in Fig. 1(c), the compressive strain of the Al-doped Ga_2O_3 nanostructures was compared to that of the thin film β-Ga_2O_3 with the same Al concentration.[29] The results revealed that substitutional Al doping in the β-Ga_2O_3 nanomaterials induced a higher compressive strain than in the thin film, presumably due to the higher surface energy in the nanomaterials. Fig. 1(d) shows the average domain sizes of the Al-doped β-Ga_2O_3 nanostructures with Al doping concentrations, showing that the normalized domain size decreased down to 65% at the Al concentration of 3.2 at%. The decrease of the domain size with the Al doping concentration was related to the lattice mismatch in the Al-doped β-Ga_2O_3 nanostructures. The crystallographic defects and/or disorders presumably enhanced the nucleation site density during the crystallization process, reducing the domain size. In addition, the Al dopants in the β-Ga_2O_3 nanostructures were able to affect the crystal growth of certain crystal faces, affecting the nanostructure shape and size. The normalized intensity and domain size in Fig. 1(b and d) are inversely proportional to the crystallographic and GBs-induced defects, respectively. Those defects were able to generate additional deep level states in the bandgap that could act as recombination centers of the charged carriers,[40] which will be correlated with the photocatalytic activity in Fig. 6 and 7.

The SEM images of the β-Ga_2O_3 nanostructures with Al concentrations are presented in Fig. 2(a–e). The intrinsic β-Ga_2O_3 nanostructures presented a spindle-like morphology with an average length of 1.25 μm. This morphology, often observed in hydrothermal synthesized Ga_2O_3 nanostructures,[41,42] morphed into nanorod structures with an average length of 0.8 μm at the Al concentration of 3.2 at%, as shown in Fig. 2(a–e). The pH value of the precursor solution for the intrinsic β-Ga_2O_3 nanostructures was initially 10.34 and gradually decreased, as summarized in Fig. 2(f). The reduction

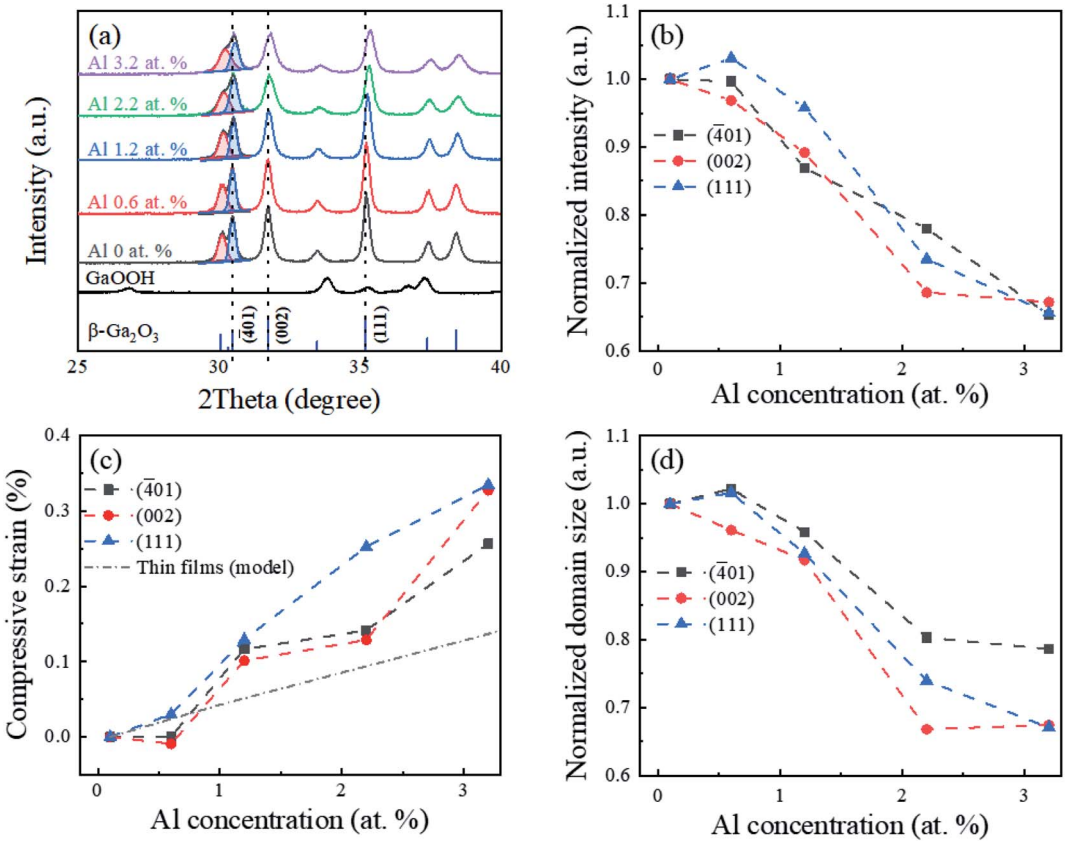

Fig. 1 (a) XRD patterns of GaOOH and β-Ga_2O_3 nanostructures with different Al concentrations; the bottom ticks indicate PDF Card No. 01-076-0573 for β-Ga_2O_3. (b) Normalized peak intensity, (c) compressive strain, and (d) normalized domain size of (−401), (002), and (111) planes as a function of Al concentrations. The compressive strain in this work was compared with that of the thin film (model).[29]

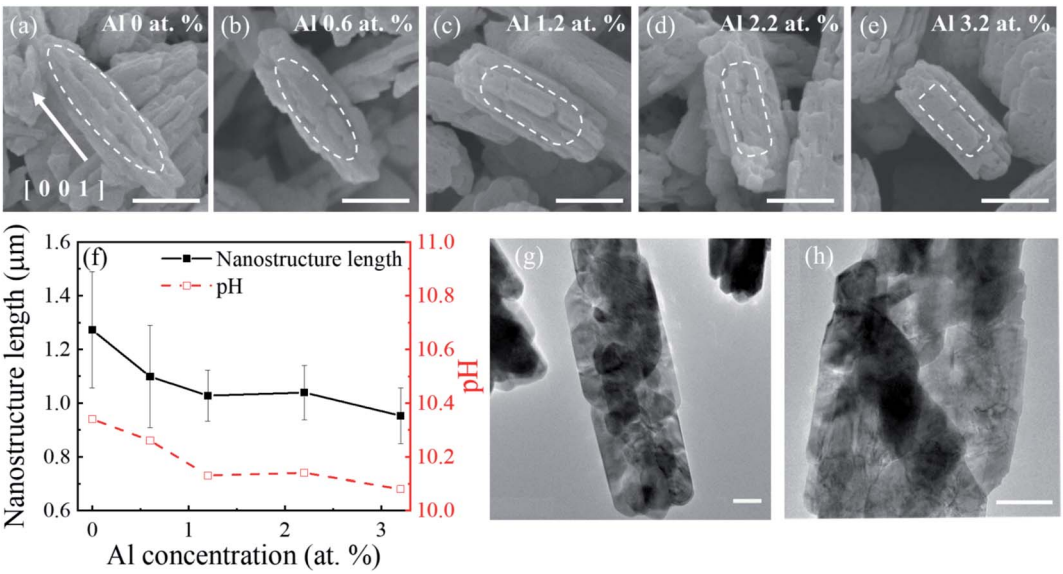

Fig. 2 (a–e) SEM images (scale bar: 500 nm) and (f) average length of β-Ga_2O_3 nanostructures with increasing Al concentrations. TEM images (scale bar: 100 nm) of (g) GaOOH nanostructures (before annealing) and (h) β-Ga_2O_3 nanostructures (after annealing) without Al doping.

of the pH in the precursor solution with the Al concentration was believed to have changed the spindle-like morphology to the nanorod structures and reduce the length as well. These results were consistent with those in previous studies.[42] This implied that the Al atoms in the β-Ga_2O_3 nanostructures and/or pH variation in the mixed solution were involved in the nucleation growth during the hydrothermal process. Fig. 2(g and h) show TEM images of the synthesized GaOOH (before annealing) and the corresponding β-Ga_2O_3 of the spindle-like morphology (after annealing) without Al dopants, respectively. The synthesized GaOOH of the orthorhombic structure consisted of well-stacked nanoplates, which transformed into the rough-surface monoclinic β-Ga_2O_3 after Ostwald's ripening (annealing).[43]

The specific surface area of the Al-doped Ga_2O_3 nanostructures was investigated using the BET method, as shown in Fig. 3. In Fig. 3(b), the surface area remains almost unchanged at around 7.4–7.6 $m^2\ g^{-1}$ within the Al range of 0–1.2 at%, and then increases with the Al concentrations. The increase of the specific surface area at the higher Al concentrations could be explained with the morphology change from the spindle-like morphology to the microrod structure along with the length reduction, as shown in Fig. 2. Higher specific surface areas are beneficial for photocatalytic reactions because the redox reactions occur on the photocatalyst surface, which would be correlated with the photocatalytic activity in Fig. 6.

The core-level spectra of the Ga 2p, Al 2p, and O 1s orbitals of the intrinsic β-Ga_2O_3 nanostructures are compared with those of Al-doped β-Ga_2O_3 nanostructures for the different Al concentrations in Fig. 4. The binding energy (BE) of the Ga^{3+} (Ga_2O_3) $2p_{3/2}$ peaks in the intrinsic β-Ga_2O_3 nanostructures was 1117.4 eV in Fig. 3(a), which was attributed to Ga–O bonding. The additional peak at 1119.1 eV was observed and its intensity

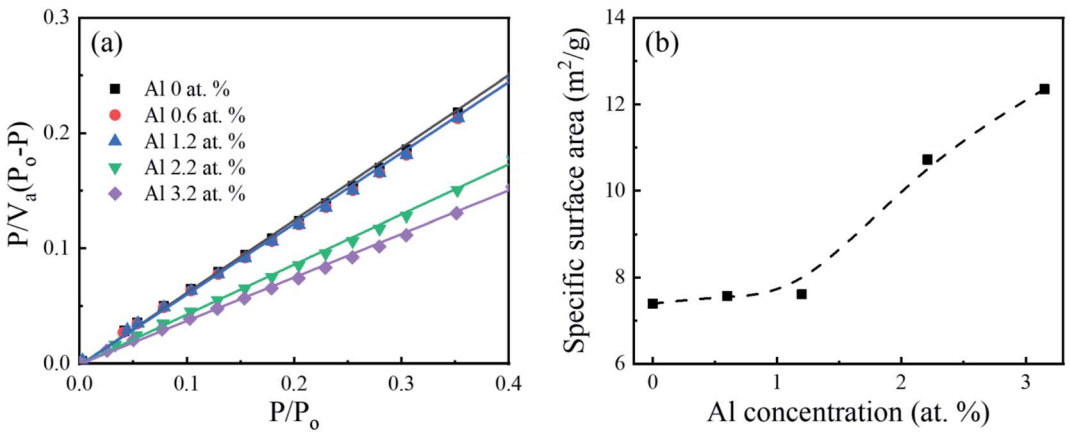

Fig. 3 (a) BET surface area plot for Al-doped Ga_2O_3 nanostructures with different Al concentrations and (b) specific surface area as a function of Al concentrations; V_a, P_o, P, and P/P_o are the adsorbed gas quantity, saturation pressure of the adsorbate, equilibrium pressure of the adsorbate, and relative pressure, respectively.

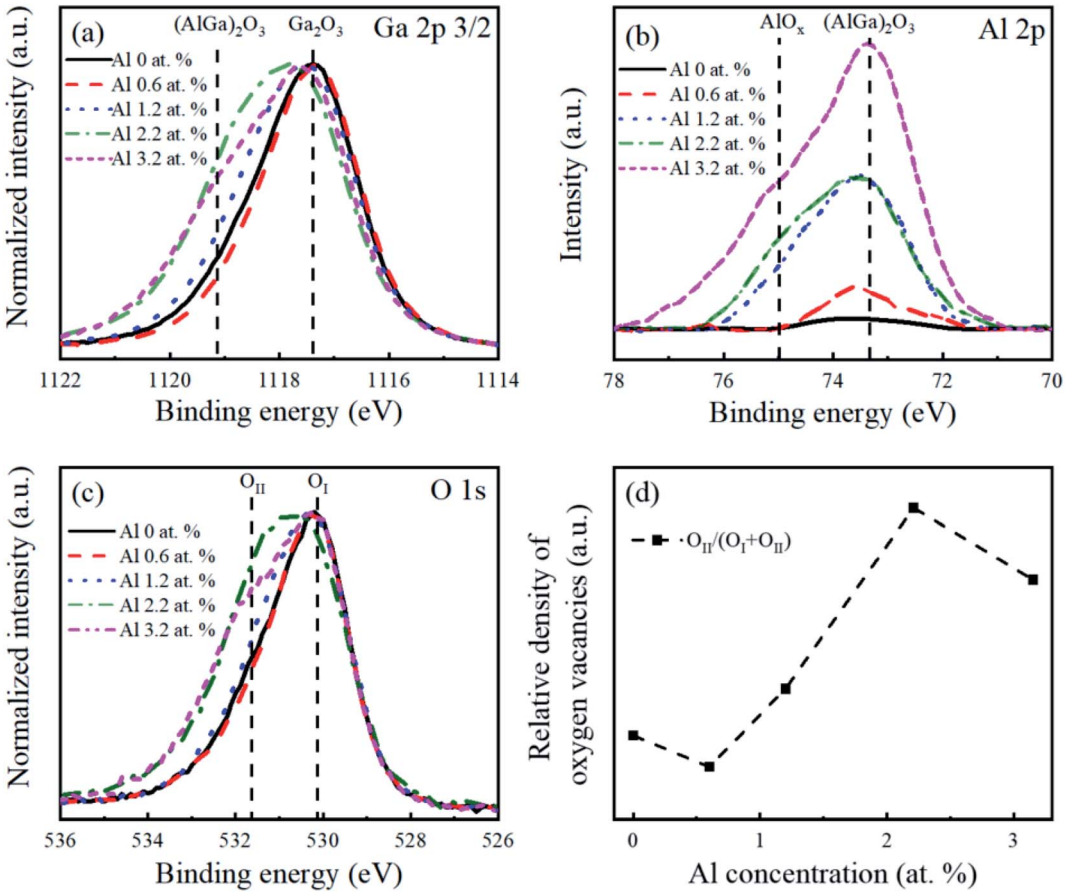

Fig. 4 XPS analysis of β-Ga_2O_3 nanostructures with different Al concentrations: core-level spectra of (a) Ga $2p_{3/2}$, (b) Al 2p, and (c) O 1s. The XPS intensity in (a and c) is normalized to increase clarity. (d) Relative intensity of $O_{II}/(O_I + O_{II})$ in O 1s spectra as a function of Al concentrations. The peak energies were calibrated using an adventitious C 1s of 284.68 eV.

increased with the Al concentration. The peak at 1119.1 eV was assigned to $(AlGa)_2O_3$ because it was higher than the G–O peak, as with the previous result.[44] The intensity of the Al 2p peak increased as the Al concentration increased, as shown in Fig. 4(b). The Al 2p peak for the 0.6 at% Al-doped β-Ga_2O_3 nanostructures was located at 73.3 eV, indicating the formation of $(AlGa)_2O_3$. As the Al concentration increased, the additional peak at 75 eV appeared, which was considered to be Al–O bonds.[30,45,46] This Al–O peak shifted toward the higher binding energy with the Al concentration in the β-Ga_2O_3, which was also in good agreement with previous reports.[30,46,47] The presence of Al–O bonding in the Al-doped β-Ga_2O_3 nanostructures presumably originated from the hydrothermal solution because the formation of $[Al(OH)_2\ aq^+]$ and $[AlO_2\ aq^-]$ was thermodynamically favorable; the Gibbs free energies of the $[Al(OH)_2\ aq^+]$ and $[AlO_2\ aq^-]$ were calculated as −914.2 and −830.9 kJ mol^{-1}, respectively.[47] In Fig. 4(c), two O 1s peaks located at 530.2 eV (O_I) and 532.0 eV (O_{II}) represented the O_2^- ions in the oxygen-saturated and oxygen-deficient regions, respectively.[48] The density of the oxygen vacancies represented by the intensity ratio of $O_{II}/(O_I + O_{II})$ is plotted in Fig. 4(d). This indicates that the small amount of Al doping (0.6 Al at%) reduced the number of oxygen-deficient defects in the Al-doped β-Ga_2O_3 nanostructures. Meanwhile, the defect density tended to increase with Al concentration when the Al concentration exceeded 0.6 at% in Fig. 4(d). This indicated that the low Al concentration (0.6 at%) in the β-Ga_2O_3 nanostructures healed the oxygen defects rather than generate additional oxygen defects.

Fig. 5(a) shows the optical absorbance and Tauc plots (direct bandgap model) of the Al-doped β-Ga_2O_3 nanostructures with different Al concentrations. The optical bandgaps of the Al-doped β-Ga_2O_3 nanostructures were obtained using a linear extrapolation from their Tauc plots and compared with those of the Al-doped β-Ga_2O_3 thin films, as shown in Fig. 5(b). The extracted optical bandgap energy of the intrinsic β-Ga_2O_3 nanostructures was ∼4.69 eV, and the bandgap energy increased with the Al concentration. This increase in the bandgap with the Al concentration was mainly caused by the increase in the conduction band edge compared with the changes in the valence band edge.[28–30] The redox potential (reduction ability) could be enhanced with the increase in the Al concentration and consequently improve the photocatalytic activity of the β-Ga_2O_3. The nanostructure bandgap was smaller than that of the thin films by around 0.2 eV, which was attributed to the light scattering effect in the nanostructures.[49]

Fig. 6(a and b) show the absorbance spectra of the MB solutions and corresponding photocatalytic activity of the β-Ga_2O_3 nanostructures as a function of Al concentration,

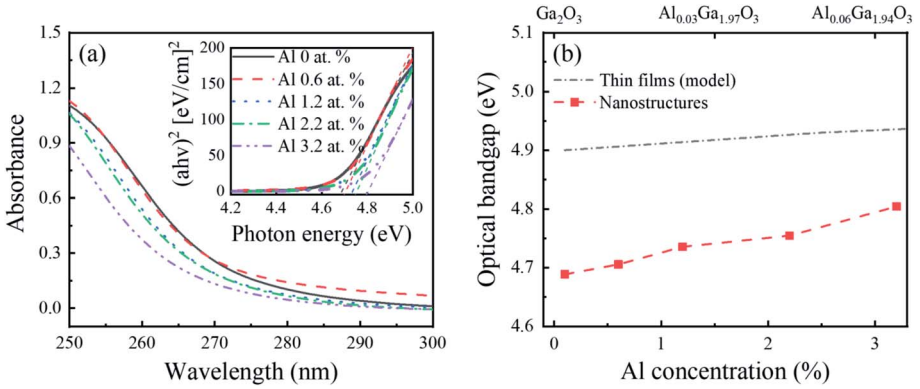

Fig. 5 (a) Optical absorbance spectra and Tauc plots (direct bandgap model) and (b) corresponding optical bandgap of the β-Ga_2O_3 nanostructures with different Al concentrations; α is the absorption coefficient, h is the Planck constant, and ν is the frequency of the electromagnetic radiation. The optical bandgap of the Al-doped β-Ga_2O_3 nanostructures is compared with that of the Al-doped β-Ga_2O_3 thin films.[29]

respectively. The photocatalytic activity of the intrinsic β-Ga_2O_3 nanostructures was ~62%, and this value increased significantly up to 88% with the Al (0.6 at%) doping in the β-Ga_2O_3 nanostructures. However, when the Al concentration further increased within the Al range of 0.6–3.2 at%, the photocatalytic activity decreased. It is noted that this degradation of MB solution was not affected by the pH value in the range of 8.0 to 10.5.[50] Fig. 6(b) also shows the Al dopant effect on the redox potential, surface area, crystallographic defects, oxygen defects, and GB-induced defects, and their correlation with the photocatalytic activity. The redox potential and surface area increased as the Al concentration increased in Fig. 6(b). Although photocatalytic activity was expected to enhance as the redox potential[51–53] and surface area[9,13] increased, the photocatalytic activity continued to decrease with Al concentration (0.6 to 3.2 at%) in this work. It indicated that apart from the redox potential and surface area, other factors dominated the photocatalytic activity of the Al-doped β-Ga_2O_3 nanostructures. Meanwhile, defects in the photocatalysts can either enhance or degrade the photocatalytic activity by acting as carrier separation and recombination sites, respectively.[54–56] Fig. 6(b) shows that as the Al concentration increased (0.6 to 3.2 at%), the crystallographic, oxygen, and GB-related defects continued to increase but accordingly the photocatalytic activity continued to decrease. The results indicated that the substituted Al atoms in the β-Ga_2O_3 nanostructures generated the crystallographic, oxygen, and GB-related defects that acted as charge recombination sites and degraded the photocatalytic activity consequently. However, this could not explain the significant enhancement of photocatalytic activity with the small amount of Al (0.6 at%) doping in the β-Ga_2O_3 nanostructures. We presumed that the amount of Al concentration is important factor for photocatalytic activity and hypothesized that when the small amount of Al atoms (0.6 at%) was doped in the Ga_2O_3, the shallow trap sites were introduced to the forbidden bands due to the dopant-induced oxygen vacancy, as shown in Fig. 7(a). These defects could retard the recombination process by separating the photogenerated electron–hole pairs, which thereby enhanced the photocatalytic activity. On the other hand, once the Al concentration in the Ga_2O_3 exceeded 0.6 at%, the crystallographic disorder, oxygen vacancy, and GB-related defects increased as the Al concentration increased. These defect-

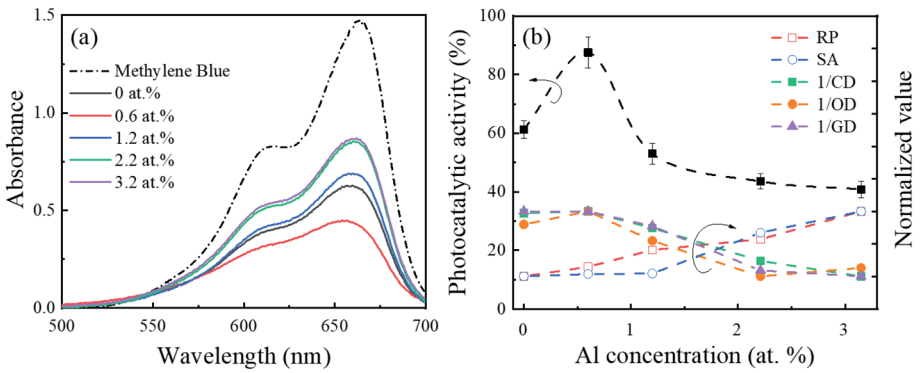

Fig. 6 (a) Absorbance spectra of the MB solution and (b) photocatalytic activity of the β-Ga_2O_3 nanostructures as a function of Al concentration under UVC irradiation for 10 min at room temperature. The error bars in the photocatalytic performance are graphical representations of a standard deviation of triple measurements. The photocatalytic activity is correlated with different parameters affecting the photocatalytic reactions, which are normalized, and the sensitivity factor is not considered; RP, SA, CD, OD, and GD represent the redox potential (Fig. 5(b)), surface area (Fig. 3(b)), crystallographic defects (Fig. 1(b)), oxygen defects (Fig. 4(d)), and GB-induced defects (Fig. 1(d)), respectively.

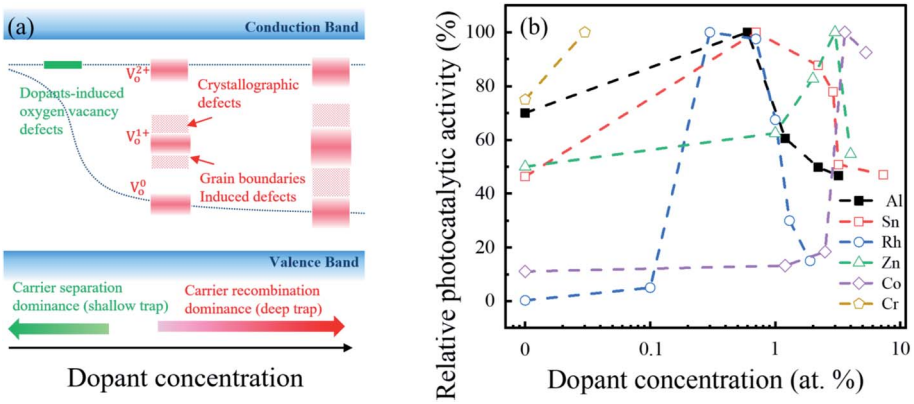

Fig. 7 (a) Trap site distribution as a function dopant concentration. The deep trap levels are generated due to the GB/crystallography[57,58,60] and oxygen vacancy[59] defects. (b) Benchmark of relative photocatalytic activity of Ga_2O_3 with different dopants and concentrations; Al and Sn *via* MB degradation under 254 nm,[26] Cr *via* Rhodamine B (RhB) degradation under 254 nm,[17] Co *via* Congo red (CR) degradation under 254 nm,[61] Zn *via* gas conversion under 254 nm,[18] and Rh *via* CO_2 conversion under 300 nm.[16]

related energy levels could be broadly distributed within the bandgap, as shown in Fig. 7(a), and acted as carrier recombination centers,[57–59] which degraded the photocatalytic activity.

Fig. 7(b) shows the relative photocatalytic activities of the β-Ga_2O_3 nanostructure for different doping materials and concentrations.[16–18,26,57–61] This comparison revealed that the photocatalytic performance of the given Ga_2O_3-based photocatalyst increased at certain small amounts of dopants, but decreased with large amounts of dopants. Therefore, an optimal balance between charge separation and recombination *via* doping approaches is important for Ga_2O_3-based photocatalyst.

Conclusion

The photocatalytic activity of Al-doped β-Ga_2O_3 nanostructures was investigated at different Al concentrations within the Al range of 0–3.2 at%. The single phase of the β-Ga_2O_3 was maintained without intermediate phases up to Al 3.2 at% doping. As the Al concentration in the β-Ga_2O_3 nanostructures increased, the optical bandgap energy of the Al-doped β-Ga_2O_3 nanostructures increased. With a small amount of substitutional Al (0.6 at%) doping in the β-Ga_2O_3 nanostructures, the degree of crystallinity, compressive strain, domain size, surface area, and oxygen defects remained unchanged, but they significantly changed as the Al concentration further increased beyond 0.6 at%. The photocatalytic activity was enhanced by doping a small amount of substitutional Al atoms (0.6 at%), which was attributed to the presence of the shallow trap level in the band gap. These shallow-level defects retarded the recombination process by separating photogenerated electron–hole pairs and thereby enhanced the photocatalytic activity. On the other hand, once the Al concentration in the Ga_2O_3 exceeded 0.6 at%, the crystallographic disorder, oxygen vacancy, and GB-related defects increased as the Al concentration increased. These defect-related energy levels could be broadly distributed within the bandgap, which acted as carrier recombination centers and consequently degraded the photocatalytic activity. The photocatalytic activity of the Al-doped β-Ga_2O_3 nanostructures was strongly correlated with the recombination process rather than the surface area and redox potential. To further enhance the photocatalytic activity of Ga_2O_3-based nanostructures, a small amount of doping without causing noticeable crystal and oxygen defects is recommended.

Conflicts of interest

There are no conflicts to declare.

Acknowledgements

This work was funded by the National Research Foundation of Korea (NRF) through the Basic Science Research Program (2017R1A2B4012278), by the Center for Advanced Soft-Electronics funded by the Ministry of Science, ICT and Future Planning, through the Global Frontier Project (CASE-2011-0031638), and by the BK21 FOUR program through the National Research Foundation of Korea (NRF) funded by the Korean government (grant number: 5199990714521). The SEM/EDS and XRD analyses were conducted at the Korea Basic Science Institute (Busan Center).

References

1 R. Roy, V. G. Hill and E. F. Osborn, Polymorphism of Ga_2O_3 and the System Ga_2O_3–H_2O, *J. Am. Chem. Soc.*, 1952, **74**, 719–722.
2 S. J. Pearton, J. Yang, P. H. Cary, F. Ren, J. Kim, M. J. Tadjer and M. A. Mastro, A review of Ga_2O_3 materials, processing, and devices, *Appl. Phys. Rev.*, 2018, **5**(1), 011301.
3 B. Fu, Z. Jia, W. Mu, Y. Yin, J. Zhang and X. Tao, A review of β-Ga_2O_3 single crystal defects, their effects on device performance and their formation mechanism, *J. Semicond.*, 2019, **40**(1), 011804.
4 D. Guo, Q. Guo, Z. Chen, Z. Wu, P. Li and W. Tang, Review of Ga_2O_3 based optoelectronic devices, *Mater. Today Phys.*, 2019, **11**, 100157.

5 Y. Yao, L. A. M. Lyle, J. A. Rokholt, S. Okur, G. S. Tompa, T. Salagaj, N. Sbrockey, R. F. Davis and L. M. Porter, Growth and characterization of α-, β-, and ε-Ga_2O_3 epitaxial layers on sapphire, *ECS Trans.*, 2017, **80**(7), 191.

6 A. Kudo and I. Mikami, Photocatalytic activities and photophysical properties of $Ga_{2-x}In_xO_3$ solid solution, *J. Chem. Soc., Faraday Trans.*, 1998, **94**(19), 2929–2932.

7 Y. Takashi, Y. Sakata and H. Imamura, Photocatalytic Decomposition of H_2O into H_2 and O_2 over Ga_2O_3 Loaded with NiO, *Chem. Lett.*, 2004, **33**(6), 726–727.

8 H. J. Yoon, J. H. Yang, S. J. Park, C. K. Rhee and Y. Sohn, Photocatalytic CO_2 reduction and hydrogen production over Pt/Zn-embedded β-Ga_2O_3 nanorods, *Appl. Surf. Sci.*, 2021, **536**, 147753.

9 Y. Hou, X. Wang, L. Wu, Z. Ding and X. Fu, Efficient decomposition of benzene over a β-Ga_2O_3 photocatalyst under ambient conditions, *Environ. Sci. Technol.*, 2006, **40**(18), 5799–5803.

10 H. J. Bae, T. H. Yoo, S. Kim, W. Choi, Y. S. Song, D. K. Kwon, B. J. Cho and W. S. Hwang, Enhanced Photocatalytic Degradation of 2-Butanone Using Hybrid Nanostructures of Gallium Oxide and Reduced Graphene Oxide Under Ultraviolet-C Irradiation, *Catalysts*, 2019, **9**(5), 449.

11 M. Akatsuka, Y. Kawaguchi, R. Itoh, A. Ozawa, M. Yamamoto, T. Tanabe and T. Yoshida, Preparation of Ga_2O_3 photocatalyst highly active for CO_2 reduction with water without cocatalyst, *Appl. Catal., B*, 2020, **262**, 118247.

12 F. Du, D. Yang, Y. Sun, Y. Jiao, F. Teng and H. Fan, Electrospun Zn-doped Ga_2O_3 nanofibers and their application in photodegrading rhodamine B dye, *Ceram. Int.*, 2020, **47**(4), 4963–4971.

13 T. H. Yoo, H. Ryou, I. G. Lee, J. Cho, B. J. Cho and W. S. Hwang, Comparison of Ga_2O_3 and TiO_2 Nanostructures for Photocatalytic Degradation of Volatile Organic Compounds, *Catalysts*, 2020, **9**(12), 545.

14 C. D. Valentin and G. Pacchioni, Spectroscopic properties of doped and defective semiconducting oxides from hybrid density functional calculations, *Acc. Chem. Res.*, 2014, **47**(11), 3233–3241.

15 D. G. Calatayud, T. Jardiel, M. Peiteado, F. Illas, E. Giamello, F. J. Palomares, D. Fernández-Hevia and A. C. Caballero, Synthesis and characterization of blue faceted anatase nanoparticles through extensive fluorine lattice doping, *J. Phys. Chem. C*, 2015, **119**(36), 21243–21250.

16 S. Kikkawa, K. Teramura, H. Asakura, S. Hosokawa and T. Tanaka, Development of Rh-Doped Ga_2O_3 Photocatalysts for Reduction of CO_2 by H_2O as an Electron Donor at a More than 300 nm Wavelength, *J. Phys. Chem. C*, 2018, **122**(37), 21132–21139.

17 L. Li, K. Xu, Y. Wang, Z. Hu and H. Zhao, Enhanced persistent luminescence and photocatalytic properties of Ga_2O_3: Cr^{3+} by In^{3+} doping, *Opt. Mater. Express*, 2016, **6**(4), 1122–1130.

18 X. Wang, S. Shen, S. Jin, J. Yang, M. Li, X. Wang, H. Hana and C. Li, Effects of Zn^{2+} and Pb^{2+} dopants on the activity of Ga_2O_3-based photocatalysts for water splitting, *Phys. Chem. Chem. Phys.*, 2013, **15**(44), 19380–19386.

19 X. Qiu, J. Zhang, H. Dong and X. Zhou, Theoretical study of metal-doped β-Ga_2O_3 photocatalysts for overall water splitting, *Theor. Chem. Acc.*, 2017, **136**(7), 79.

20 Y. Ma, X. Zhao, M. Niu, W. Li, X. Wang, C. Zhai, T. Wang, Y. Tang and X. Dai, Monoclinic Ga_2O_3 (100) surface as a robust photocatalyst for water-splitting, *RSC Adv.*, 2017, **7**(7), 4124–4134.

21 J. Ding, L. Zhong, X. Wang, L. Chai, Y. Wang, M. Jiang, T. T. Li, Y. Hu, J. Qian and S. Huang, General approach to MOF-derived core-shell bimetallic oxide nanowires for fast response to glucose oxidation, *Sens. Actuators, B*, 2020, **306**, 127551.

22 Y. Mei, T. T. Li, J. Qian, H. Li and Y. Q. Zheng, Improved performance of photoelectrochemical water oxidation from nanostructured hematite photoanode with an immobilized molecular cobalt salophen catalyst, *J. Mater. Sci.*, 2020, **55**(27), 12864–12875.

23 Q. Zhou, T. T. Li, J. Qian, Y. Hu, F. Guo and Y. Q. Zheng, Self-supported hierarchical CuO_x@ Co_3O_4 heterostructures as efficient bifunctional electrocatalysts for water splitting, *J. Mater. Chem. A*, 2018, **6**(29), 14431–14439.

24 S. Zhu and D. Wang, Photocatalysis: basic principles, diverse forms of implementations and emerging scientific opportunities, *Adv. Energy Mater.*, 2017, **7**(23), 1700841.

25 R. S. Varma, N. Thorat, R. Fernandes, D. C. Kothari, N. Patela and A. Miotellob, Dependence of photocatalysis on charge carrier separation in Ag-doped and decorated TiO_2 nanocomposites, *Catal. Sci. Technol.*, 2016, **6**(24), 8428–8440.

26 H. Ryou, T. H. Yoo, Y. Yoon, I. G. Lee, M. Shin, J. Cho, B. J. Cho and W. S. Hwang, Hydrothermal Synthesis and Photocatalytic Property of Sn-doped β-Ga_2O_3 Nanostructure, *ECS J. Solid State Sci. Technol.*, 2020, **9**, 045009.

27 T. H. Yoo, H. Ryou, I. G. Lee, B. J. Cho and W. S. Hwang, Enhanced Photocatalytic Activity of Electrospun β-Ga_2O_3 Nanofibers *via In Situ* Si Doping Using Tetraethyl Orthosilicate, *Catalysts*, 2019, **9**(12), 1005.

28 T. Wang, W. Li, C. Ni and A. Janotti, Band gap and band offset of Ga_2O_3 and $(Al_xGa_{1-x})_2O_3$ alloys, *Phys. Rev. Appl.*, 2018, **10**(1), 011003.

29 H. Peelaers, J. B. Varley, J. S. Speck and C. G. Van de Walle, Structural and electronic properties of Ga_2O_3–Al_2O_3 alloys, *Appl. Phys. Lett.*, 2018, **112**(24), 242101.

30 F. Zhang, C. Hu, M. Arita, K. Saito, T. Tanaka and Q. Guo, Low temperature growth of $(AlGa)_2O_3$ films by oxygen radical assisted pulsed laser deposition, *CrystEngComm*, 2020, **22**(1), 142–146.

31 H. J. Bae, T. H. Yoo, Y. Yoon, I. G. Lee, J. P. Kim, B. J. Cho and W. S. Hwang, High-Aspect Ratio β-Ga_2O_3 Nanorods *via* Hydrothermal Synthesis, *Nanomaterials*, 2018, **8**(8), 594.

32 T. Sato and T. Nakamura, Studies of the crystallisation of gallium hydroxide precipitated from hydrochloric acid solutions by various alkalis, *J. Chem. Technol. Biotechnol.*, 1982, **32**(3), 469–475.

33 G. Zhang, Y. Li and Y. Wu, pH controlled synthesis of UV excited host-sensitized luminescence in Dy^{3+} doped Ga_2O_3, *J. Lumin.*, 2019, **212**, 29–37.

34 A. L. Patterson, The Scherrer formula for X-ray particle size determination, *Phys. Rev.*, 1939, **56**(10), 978.
35 Z. Wang, H. Zhao, H. Qi, X. Liu and Y. Liu, Free radical behaviours during methylene blue degradation in the Fe^{2+}/H_2O_2 system, *Environ. Technol.*, 2019, **40**(9), 1138–1145.
36 Y. Nosaka and A. Y. Nosaka, Generation and detection of reactive oxygen species in photocatalysis, *Chem. Rev.*, 2017, **117**(17), 11302–11336.
37 M. Mizuno, T. Yamada and T. Noguchi, The Liquidus Curve in the System Al_2O_3–Ga_2O_3 as Measured with a Solar Furnace, *J. Ceram. Assoc. Jpn.*, 1975, **83**, 175–177.
38 F. P. Sabino, L. N. de Oliveira and J. L. F. Da Silva, Role of atomic radius and d-states hybridization in the stability of the crystal structure of M_2O_3 (M= Al, Ga, In) oxides, *Phys. Rev. B: Condens. Matter Mater. Phys.*, 2014, **90.15**, 155206.
39 J. Emsley, *The Elements*, 3rd edn, Clarendon Press, Oxford, U.K., 1998.
40 J.-L. Maurice, On the origin of the electrical activity in silicon grain boundaries, *Rev. Phys. Appl.*, 1987, **22**(7), 613–621.
41 J. Zhang, S. Jiao, Y. Wan, S. Gao, D. Wang and J. Wang, A well-grown β-Ga_2O_3 microrod array formed from GaOOH on a Si (100) substrate and growth mechanism study, *CrystEngComm*, 2018, **20**, 4329–4335.
42 Y. Zhao, R. L. Frost, J. Yang and W. N. Martens, Size and Morphology Control of Gallium Oxide Hydroxide GaO(OH), Nano- to Micro-Sized Particles by Soft-Chemistry Route without Surfactant, *J. Phys. Chem. C*, 2008, **112**, 3568–3579.
43 L. S. Reddy, Y. H. Ko and J. S. Yu, Hydrothermal Synthesis and Photocatalytic Property of β-Ga_2O_3 Nanorods, *Nanoscale Res. Lett.*, 2015, **10**, 364.
44 Q. Feng, X. Li, G. Han, L. Huang, F. Li, W. Tang, J. Zhang and Y. Hao, $(AlGa)_2O_3$ solar-blind photodetectors on sapphire with wider bandgap and improved responsivity, *Opt. Mater. Express*, 2017, **7**, 1240–1248.
45 F. Zhang, K. Saito, T. Tanaka, M. Nishio, M. Arita and Q. Guo, Wide bandgap engineering of $(AlGa)_2O_3$ films, *Appl. Phys. Lett.*, 2014, **105**, 162107.
46 Z. Hu, Q. Feng, J. Zhang, F. Li, X. Li, Z. Feng, C. Zhang and Y. Hao, Optical properties of $(AlxGa_{1-x})_2O_3$ on sapphire, *Superlattices Microstruct.*, 2018, **114**, 82–88.
47 B. S. Hemingway, R. A. Robie and J. A. Kittrick, Revised values for the Gibbs free energy of formation of [$Al(OH)_4$ aq^-], diaspore, boehmite and bayerite at 298.15 K and 1 bar, the thermodynamic properties of kaolinite to 800 K and 1 bar, and the heats of solution of several gibbsite samples, *Geochim. Cosmochim. Acta*, 1978, **42**, 1533–1543.
48 S. Yuan, S. Ou, S. Huang and D. Wuu, Enhanced Deep-Ultraviolet Responsivity in Aluminum–Gallium Oxide Photodetectors *via* Structure Deformation by High-Oxygen-Pressure Pulsed Laser Deposition, *ACS Appl. Mater. Interfaces*, 2019, **11**, 17563–17569.
49 Y. Yoon, K. I. Han, B. H. Kim, I. G. Lee, Y. Kim, J. P. Kim and W. S. Hwang, Formation of β-Ga_2O_3 nanofibers of sub-50 nm diameter synthesized by electrospinning method, *Thin Solid Films*, 2018, **645**, 358–362.
50 H. Ryou, S. Kim, M. Shin, J. Cho and W. S. Hwang, Fast-Response Colorimetric UVC Sensor Made of a Ga_2O_3 Photocatalyst with a Hole Scavenger, *Sensors*, 2021, **21**, 387.
51 M. Haruta, Size- and support-dependency in the catalysis of gold, *Catal. Today*, 1997, **36**, 153–166.
52 S. Panigrahi, S. Basu, S. Praharaj, S. Pande, S. Jana, A. Pal, S. K. Ghosh and T. Pal, Synthesis and Size-Selective Catalysis by Supported Gold Nanoparticles: Study on Heterogeneous and Homogeneous Catalytic Process, *J. Phys. Chem. C*, 2007, **111**, 4596–4605.
53 P. Liu, R. Qin, G. Fu and N. Zheng, Surface Coordination Chemistry of Metal Nanomaterials, *J. Am. Chem. Soc.*, 2017, **139**, 2122–2131.
54 W. Zhou and H. Fu, Defect-mediated electron–hole separation in semiconductor photocatalysis, *Inorg. Chem. Front.*, 2018, **5**, 1240–1254.
55 J. Liu, Z. Wei and W. Shangguan, Defects Engineering in Photocatalytic Water Splitting Materials, *ChemCatChem*, 2019, **11**, 6177–6189.
56 M. Montero-Muñoz, J. E. Ramos-Ibarra, J. E. Rodríguez-Páez, M. D. Teodoro, G. E. Marques, A. R. Sanabria, P. C. Cajas, C. A. Páez, B. Heinrichs and J. A. H. Coaquira, Role of defects on the enhancement of the photocatalytic response of ZnO nanostructures, *Appl. Surf. Sci.*, 2018, **448**, 646–654.
57 Y. Yan, W.-J. Yin, Y. Wu, T. Shi, N. R. Paudel, C. Li, J. Poplawsky, Z. Wang, J. Moseley, H. Guthrey, H. Moutinho, S. J. Pennycook and M. M. Al-Jassim, Physics of grain boundaries in polycrystalline photovoltaic semiconductors, *J. Appl. Phys.*, 2015, **117**(11), 112807.
58 J. Y. W. Seto, The electrical properties of polycrystalline silicon films, *J. Appl. Phys.*, 1975, **46**(12), 5247–5254.
59 H. Liang, S. Cui, R. Su, P. Guan, Y. He, L. Yang, L. Chen, Y. Zhang, Z. Mei and X. Du, Flexible X-ray Detectors Based on Amorphous Ga_2O_3 Thin Films, *ACS Photonics*, 2018, **6**(2), 351–359.
60 X. Ma, Y. Zhang, L. Dong and R. Jia, First-principles calculations of electronic and optical properties of aluminum-doped β-Ga_2O_3 with intrinsic defects, *Results Phys.*, 2017, **7**, 1582–1589.
61 M. Bagheri, A. R. Mahjoub, A. A. Khodadadi and Y. Mortazavi, Fast photocatalytic degradation of congo red using CoO-doped b-Ga_2O_3 nanostructures, *RSC Adv.*, 2014, **4**(63), 33262–33268.